

Article

Carbon Stock Assessment Using Remote Sensing and Forest Inventory Data in Savannakhet, Lao PDR

Phutchard Vicharnakorn ^{1,*}, Rajendra P. Shrestha ¹, Masahiko Nagai ², Abdul P. Salam ³ and Somboon Kiratiprayoon ⁴

¹ Natural Resources Management, School of Environment, Resources, and Development, Asian Institute of Technology, P.O. Box 4, Klong Luang 12120, Thailand; E-Mail: rajendra@ait.ac.th

² Remote Sensing and GIS, School of Engineering and Technology, Asian Institute of Technology, P.O. Box 4, Klong Luang 12120, Thailand; E-Mail: nagaim01@gmail.com

³ Energy, School of Environment, Resources, and Development, Asian Institute of Technology, P.O. Box 4, Klong Luang 12120, Thailand; E-Mail: salam@ait.ac.th

⁴ School of Science and Technology, Thammasat University, 99 Paholyothin Rd., Klong Luang 12120, Thailand; E-Mail: sxk49@yahoo.com

* Author to whom correspondence should be addressed; E-Mail: armouy2002@hotmail.com; Tel.: +66-8-1361-5834; Fax: +66-2215-8914.

Received: 29 January 2014; in revised form: 29 May 2014 / Accepted: 29 May 2014 /

Published: 12 June 2014

Abstract: Savannakhet Province, Lao People's Democratic Republic (PDR), is a small area that is connected to Thailand, other areas of Lao PDR, and Vietnam via road No. 9. This province has been increasingly affected by carbon dioxide (CO₂) emitted from the transport corridors that have been developed across the region. To determine the effect of the CO₂ increases caused by deforestation and emissions, the total above-ground biomass (AGB) and carbon stocks for different land-cover types were assessed. This study estimated the AGB and carbon stocks (t/ha) of vegetation and soil using standard sampling techniques and allometric equations. Overall, 81 plots, each measuring 1600 m², were established to represent samples from dry evergreen forest (DEF), mixed deciduous forest (MDF), dry dipterocarp forest (DDF), disturbed forest (DF), and paddy fields (PFi). In each plot, the diameter at breast height (DBH) and height (H) of the overstory trees were measured. Soil samples (composite $n = 2$) were collected at depths of 0–30 cm. Soil carbon was assessed using the soil depth, soil bulk density, and carbon content. Remote sensing (RS; Landsat Thematic Mapper (TM) image) was used for land-cover classification and

development of the AGB estimation model. The relationships between the AGB and RS data (e.g., single TM band, various vegetation indices (VIs), and elevation) were investigated using a multiple linear regression analysis. The results of the total carbon stock assessments from the ground data showed that the MDF site had the highest value, followed by the DEF, DDF, DF, and PFi sites. The RS data showed that the MDF site had the highest area coverage, followed by the DDF, PFi, DF, and DEF sites. The results indicated significant relationships between the AGB and RS data. The strongest correlation was found for the PFi site, followed by the MDF, DDF, DEF, and DF sites.

Keywords: above-ground biomass; carbon stock; Landsat; vegetation indices; image classification

1. Introduction

Tropical forest lands are a natural forest type that is an important source of biodiversity, food, and carbon storage. Tropical forests comprise the largest proportion of the world's forests at 44% [1]; they also contain one of the largest carbon pools and have a significant function in the global carbon cycle. Forests store carbon and contain approximately 80% of the total above-ground organic carbon and 40% of the total below-ground organic carbon worldwide. Deforestation and forest degradation contribute 15%–20% of global carbon emissions, and most of this contribution comes from tropical regions. Approximately 60% of the carbon sequestered by forests is released back into the atmosphere via deforestation. Scientists have also determined that tropical deforestation releases 1.5 Gt of carbon into the atmosphere each year [2]. Deforestation and forest degradation are the major sources of greenhouse gas (GHG) emissions in most tropical countries. The Intergovernmental Panel on Climate Change (IPCC) [3] estimated that the global carbon dioxide (CO₂) emissions from land-use change, averaged over the 1990s, ranged between 0.5 and 2.7 Gt C·a⁻¹, with an average of 1.6 Gt C·a⁻¹.

Forest biomass is an indicator of carbon sequestration. The amount of carbon sequestered by a forest can be inferred from its biomass accumulation because approximately 50% of forest dry biomass is carbon [4]. The majority of biomass assessments are performed for the above-ground biomass (AGB) of trees because this biomass generally represents the greatest fraction of the total living biomass in a forest and does not pose significant logistical problems during field measurements [3]. Estimating above-ground forest biomass is the most important step in measuring the carbon stocks and fluxes from tropical forests and helps to determine the contribution of forests to the global carbon cycle. Moreover, estimates of AGB can also be used to predict root biomass, which is generally estimated to be 20% of the above-ground forest biomass [5]; this figure was based on a predictive relationship determined from an extensive literature review [6]. In addition, dead wood or litter carbon stocks (e.g., downed trees, standing dead or broken branches, leaves) are normally presumed to correspond to 10%–20% of the above-ground forest carbon stock in mature forests [7].

Deforestation and forest degradation continue to be an important environmental problem in Lao People's Democratic Republic (PDR). In the 1950s, forests covered approximately 70% of the land area in this country; however, by 1992, the forest coverage had declined to approximately 47% of the

total land area as a result of population expansion, agricultural cultivation, and timber exports [8]. In 2005, land-use change and forestry in Lao PDR, including deforestation and land clearing, were responsible for 26% of the GHG emissions, and transport was responsible for 9% of the emissions. These emissions are expected to increase annually. The data from the Lao PDR forest department assessments of the forest land cover in 1982 and 2010 showed that forest with more than 20% crown cover decreased from 6.04 billion to 5.15 billion tons over this 28-year period; moreover, the total volume lost between 1982 and 2010 was approximately 148 million m³. As forests can contribute to offsetting emissions, the current forest areas must be measured to ensure their protection.

Traditional biomass assessment methods based on field measurements are the most accurate methods; however, they are difficult to conduct over large areas and are costly, time consuming, and labor intensive [9]. Recently, remote-sensing (RS) procedures have been applied to and established for natural resources management. Currently, RS is widely used to collect information regarding forest AGB and vegetation structure as well as to monitor and map vegetation biomass and productivity on large scales [10–12] by measuring the spectral reflectance of the vegetation [13]. However, optical RS does not directly assess above-ground forest biomass, and radiometry is sensitive to vegetation structure (*i.e.*, crown size and tree density), texture, and shadow, which are correlated with AGB, particularly in the infrared bands [14,15]. RS data are now considered to be the most reliable method of estimating spatial biomass in tropical regions over large areas. RS technology has been applied to biomass assessment in many studies [10,16,17] because it can obtain forest information over large areas at a reasonable cost and with acceptable accuracy based on repetitive data collection with minimal effort [13].

In general, estimating the AGB in tropical forests is a challenging task because of their complex forest structure. Many studies have shown that the method of determining relationships between field measurements and RS data and then extrapolating these relationships over large areas is very useful [18]. To determine the relationship between above-ground field biomass and RS data, researchers have used linear regression models with or without log transformations of field biomass data [19,20] and multiple regressions with or without stepwise selection [13,20–22]. Artificial neural networks [20,23], semi-empirical models [24], nonlinear regression [25], and nonparametric estimation techniques (*e.g.*, *k*-nearest neighbor and *k*-means clustering) have also been used [13,26]. Although no model can determine this complex relationship absolutely, researchers continue to use multiple regression models as one of the best options. Vegetation index models are generally used to estimate biomass in many studies [20,27,28]. Vegetation indices (VIs) are calculated from mathematical transformations of the original spectral reflectance data and can be used to interpret land vegetation cover [29]. VIs are applied to remove the variations caused by spectral reflectance measurements while also measuring the biophysical properties that result from the soil background, sun view angles, and atmospheric conditions [13]. Many previous studies have shown significant positive relationships between biomass and VIs [6,30,31]; however, other studies have shown poor relationships [30,31].

Many methods can be used to map and estimate above-ground forest biomass for different land-cover types; one such method is the use of Landsat imagery (medium-resolution satellite images) to estimate the attributes of forests through direct correlations or stepwise regression analyses with spectral bands, band ratios, or VIs [11,27,32]. In general, land-cover change mapping cannot be accurately performed based on low- and medium-resolution satellite images. However, the use of

high-resolution images to map large areas is expensive and requires a high degree of technical skill for data interpretation; these issues are problematic in developing countries. Landsat is commonly used for many applications because it can be obtained for free or at a low cost. A combination of many data sources (e.g., forest inventory, land use, elevation, and RS data) can be used to predict vegetation variables over large areas [33]. A hybrid supervised/unsupervised classification approach coupled with a geographical information systems (GIS) analysis has been employed to improve land use/cover mapping for Landsat data [33–35]. In tropical regions, forest plot-based field measurements have been correlated with RS data, and these measurements have been used to estimate that carbon stocks are limited, particularly in Southeast Asian countries, such as Lao PDR. The present study seeks to characterize the carbon stock of tropical forest types using forest-plot-based field measurements and RS data to develop a simple RS-based methodology. The field-based measurement and RS approach might also help to improve forest carbon estimation in order to reduce emissions resulting from deforestation and forest degradation (REDD+) and to design incentive programs; furthermore, this approach might improve forest management with regard to climate-change mitigation.

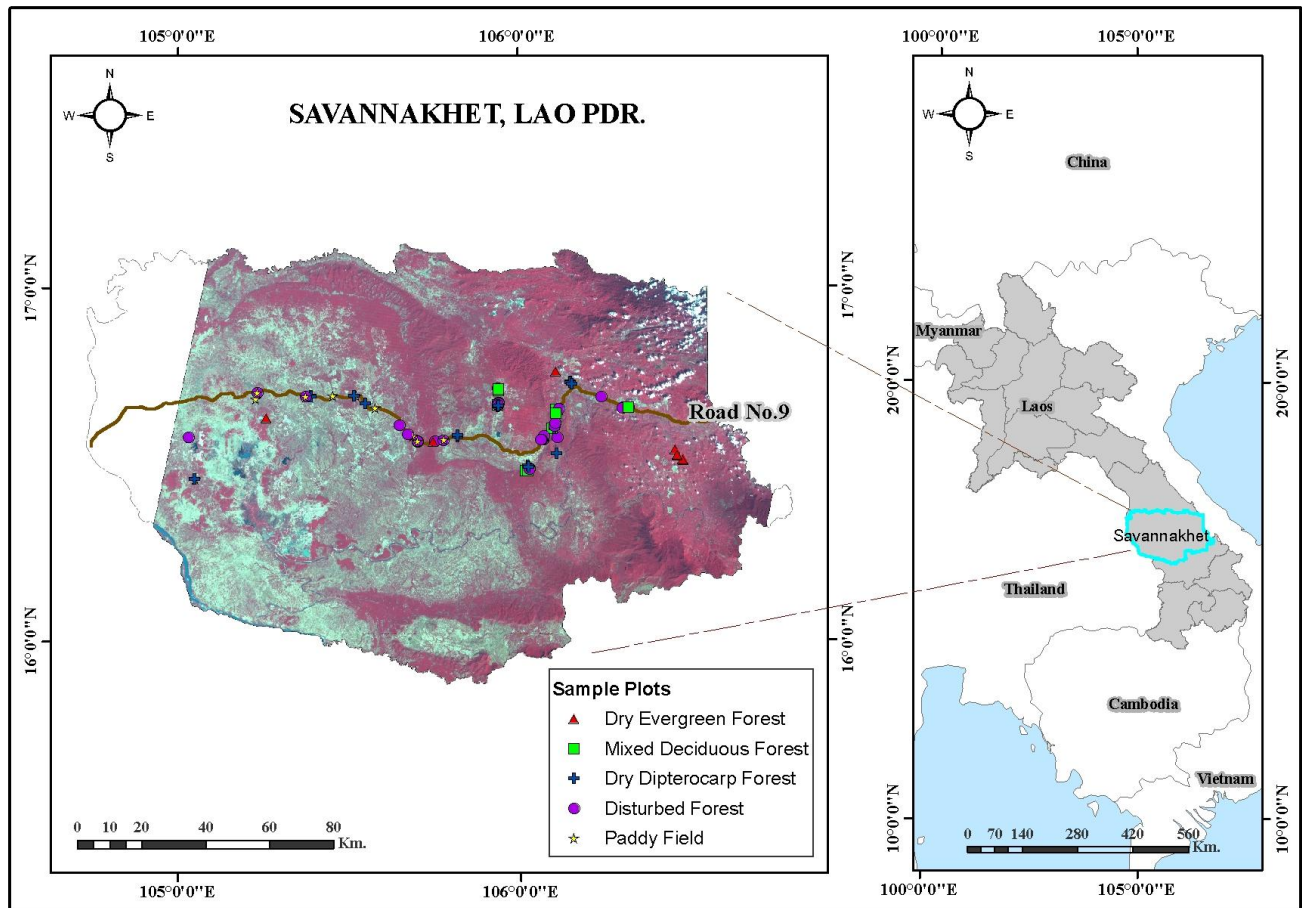
2. Methods

2.1. Study Area

Savannakhet Province is located in the southern region of Lao PDR, lying between 16° and 17° north latitude and between 105° and 106° east longitude (Figure 1). This province covers 21,774 km², and its topography is lowland with a slight slope from east to west to the Mekong River. Savannakhet Province contains the largest rice field area in the country [36], and the dominant occupation is farming. Savannakhet is connected to Thailand, other areas of Lao PDR, and Vietnam via road No. 9, and it is linked to China and Cambodia via road No. 13.

Savannakhet has a tropical monsoon climate, and the average annual temperature is 26.3 °C. The landscape varies from low-lying floodplains to foothills and mountains. The average annual rainfall is approximately 1440 mm and is significantly higher in the eastern upland region of the province than in the lower areas. Rice is a major crop in this region. Lao PDR relies on forest products because it has a low population density and a large forested area. Forest products meet a wide range of subsistence needs, provide opportunities for income generation, and are an important source of export income [37]. Savannakhet has large forested areas, including natural protected areas (Phou Xang Hae, Dong Nadet, and Don Phou Vieng) and a natural production forest (Dong Sithouane). In 2000, forest land covered approximately 70% of the province. Forestry is the second most important economic sector, after agriculture, and a key source of export income for Savannakhet [37,38]. However, Lao PDR is aware of the recent decline of its natural resources due to an increasing population, encroachments on its forests for settlement, agricultural cultivation, illegal logging, and forest fires.

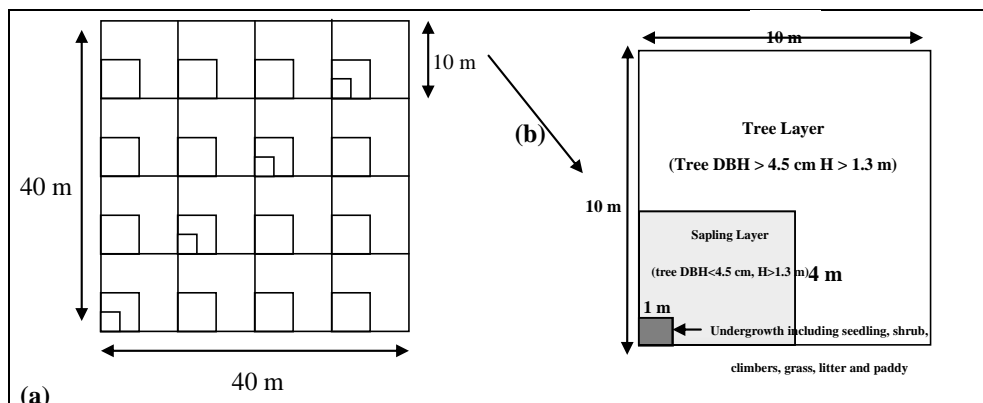
Figure 1. The location of the study area inventory plots in Savannakhet Province, Lao PDR.



2.2. Field Data Collection

The study site is located in a tropical forest containing various forest types: dry evergreen forest (DEF), mixed deciduous forest (MDF), dry dipterocarp forest (DDF), disturbed forest (DF), and paddy fields (PFi). A total of 81 field plots were located within the Savannakhet region, including 11, 10, 20, 29, and 11 plots of DEF, MDF, DDF, DF, and PFi, respectively (see Figure 1). The sample plots were primarily established along road No. 9, from 19 September to 9 October 2011. Each plot had dimensions of 40×40 m. Sampling quadrats (square plots) with dimensions of 40×40 m, 10×10 m, 4×4 m, and 1×1 m were nested within each other. The design of the plots was optimized to ensure that the area on the ground occupied at least one full Landsat TM image with a 30-m pixel resolution. For the 10×10 m quadrat (tree layer), all of the trees in all of the subplots with a diameter at breast height (DBH) equal to or greater than 4.5 cm and a height (H) greater than 1.3 m above the surface level were measured [13]. Information concerning the tree species, including the scientific names of the trees, was collected. The sapling layer of trees with a DBH less than 4.5 cm and a H greater than 1.3 m was measured in the 4×4 m quadrats of all the subplots (see Figure 2a,b). Tree species information was collected. The undergrowth layer, including seedlings, shrubs, climbers, grasses, litter (twigs and leaves), and paddy rice, was collected from four 1×1 m quadrats (Figure 2a,b). For this analysis, the undergrowth layer was weighed and dried. Soil samples were collected from two points at each site for bulk density and soil carbon content analyses for DEF, MDF, DDF, DF, and PFi.

Figure 2. (a) The 40 × 40-m quadrat design; (b) nested quadrats for biomass diversity and soil analysis.



2.3. AGB and Soil Carbon Analysis from Field Data

Forests and paddies with trees are the major types of land cover in Lao PDR. DBH and H values were recorded for all trees (DBH value ≥ 4.5 cm) and saplings (DBH value < 4.5 cm), and the AGB was estimated using the allometric equation shown in Table 1 for each land-cover type [39–42] for DEF, MDF, and DDF. All of these allometric equations can represent forest types in this study area. They were developed for vegetation in Thailand and have been used successfully in Thailand, which has similar vegetation characteristics to those of Lao PDR. The estimate of the sapling AGB was obtained from the allometric equation for DEF, MDF, and DDF. These equations are advantageous because they include a H-adjusted function. Additionally, many studies have used them to examine forest biomass for carbon stock assessment in Thailand [39–44].

Table 1. Equations used for above-ground biomass (AGB) assessment.

Land-Cover Type		Allometric Equation	Source	
Tree	DEF	$W_s = 0.0509 \text{ DBH}^2 \text{H}^{0.919}$	Tsutsumi <i>et al.</i> [39]	
		$W_b = 0.00893 \text{ DBH}^2 \text{H}^{0.977}$		
		$W_l = 0.0140 \text{ DBH}^2 \text{H}^{0.669}$		
MDF	DDF	$W_s = 0.0396 \text{ DBH}^2 \text{H}^{0.9326}$	Ogawa <i>et al.</i> [40]	
		$W_b = 0.003487 \text{ DBH}^2 \text{H}^{1.0270}$		
		$W_l = (28.0/W_{tc} + 0.025)^{-1}$		
Sapling	DEF	$W_s = 0.0702 \text{ DBH}^2 \text{H}^{0.8737}$	Visaratana and Chernkhuntod [41]	
		$W_b = 0.0093 \text{ DBH}^2 \text{H}^{0.9403}$		
		$W_l = 0.0244 \text{ DBH}^2 \text{H}^{1.0517}$		
	MDF	DDF	$W_s = 0.0893059 \text{ DBH}^2 \text{H}^{0.66513}$	Suwannapinunt [42]
			$W_b = 0.0153063 \text{ DBH}^2 \text{H}^{0.58255}$	
			$W_l = 0.0000140 \text{ DBH}^2 \text{H}^{0.44363}$	
		$W_s = \text{Biomass of stem (kg)}$		
		$W_b = \text{Biomass of branch (kg)}$		
		$W_l = \text{Biomass of leaves (kg)}$		
		Total biomass (kg) = $W_s + W_b + W_l$		
		DBH = Diameter at breast height (cm)		
		H = Tree height (m)		

The undergrowth biomass (vegetation with a H value < 1.30 m), including seedlings, shrubs, climbers, grasses, litter (twigs and leaves), and paddy rice, was estimated directly using the harvesting method. The fresh weight was measured, and the dry weight was determined by oven-drying at 70 °C for at least 48 hours in the lab before weighing. The total dry weight of the biomass was calculated from the fresh weight [45] using the equation below:

$$\text{Total DW (kg}\cdot\text{m}^{-2}) = \frac{(\text{TotalFW (kg)} \times \text{SubsampleDW (g)})}{\text{SubsampleFW (g)} \times \text{Samplearea (m}^2)} \quad (1)$$

where DW is the dry weight and FW is the fresh weight.

The AGB was converted to carbon stock by multiplying 0.47 as a conversion factor [1,3] using the equation below:

$$\text{Above-ground carbon stock} = \text{AGB} \times 0.47 \quad (2)$$

Soil was collected at two time points from two land-cover types for both the bulk density (g/cm^3) and soil carbon content (%) analyses at a depth of 30 cm (top soil) [46]. A soil auger was used to collect the soil sample. Bulk density was calculated using Equation (3) [47,48], and soil carbon content was calculated via air drying and then baking at 900 °C using an NC-Analyzer Model Sumigraph-NC 90A. The soil carbon content was calculated by multiplying the volume percentage of the soil organic carbon in the top soil horizon by the soil bulk density value (g/cm^3) and then multiplying the result by the carbon content percentage. As suggested by Black [49], the soil carbon content (t/ha) was calculated using Equation (4). The total carbon stock was calculated using Equation (5).

$$\text{Bulk Density (g}/\text{cm}^3) = \frac{\text{Mass of oven-dried soil}}{\text{Total Volume}} \quad (3)$$

$$\text{Soil carbon (t/ha)} = \text{Soil depth (cm)} \times \text{soil bulk density (g}/\text{cm}^3) \times \text{carbon content (\%)} \quad (4)$$

$$\text{Total carbon stock} = \text{Above ground carbon stock} + \text{soil carbon} \quad (5)$$

2.4. Land-Cover Classification Method

Two cloudless scenes (12648 and 12649) of Landsat TM images taken on 26 August 2009, were downloaded from the U.S. Geological Survey (USGS) [50]. The image was georectified to the universal transverse mercator (UTM) projection using image registration. All Landsat Thematic Mapper (TM) bands (except the thermal bands) were stacked, and the image was subset for the Savannakhet area as shown in Figure 1. The land-cover map was classified to estimate the biomass and carbon stock for each class using Erdas software. The classifications including DEF, MDF, DDF, DF, and PFi with trees were analyzed using a hybrid classification technique that uses both supervised and unsupervised classifications with GIS [34,51]. The hybrid classification involved developing training patterns via the use of an unsupervised classification followed by a supervised classification [51]. For the unsupervised classification, a K-means clustering algorithm was used to search for natural groups of pixels called clusters, which were located in the data by assessing the relative locations of the pixels in the feature space for separations between vegetation and non-vegetation classes. The vegetation classes were also identified for field verification in the study area. The maximum likelihood method for the supervised classification was applied using analyst-defined training areas to determine

the characteristics of each land-cover type. Clouds and shadows were filled using nearby pixels, Google Maps, land-use Shapefile data, and land-cover classifications from older and newer images. As the resolution of Landsat images is moderate (30×30 m), the use of a combined hybrid classification technique improved the accuracy of the land-cover classification [34,51]. An accuracy assessment was applied to evaluate the quality of the land cover map [34]. The accuracy of each classification was assessed by comparing the classification with the reference data. In all, 81 plots were collected. Of these plots, 41 were used for image classification; another 40 plots were used as reference data. On this basis, an error matrix was produced for each result to present the overall accuracy, the user and producer accuracy, and the kappa coefficient.

2.5. The Correlation between AGB and RS Data

In the current study, the relationship between AGB and RS data was assessed based on field measurements of each vegetation class. In a previous study, TM spectral bands and VIs were tested for their ability to predict AGB. Using TM spectral bands or VIs alone was not sufficient to establish effective AGB estimates [52]. In the current study, RS data and the reflectance of six individual bands (blue, green, red, near-infrared (NIR), and two middle-infrared (MIR)), as well as various VIs and elevation data were tested to determine their relationships with AGB using field plot data for various types of land cover. The forest inventory plots were identified using GPS. The locations of the forest inventory plots were overlaid on the RS data. The elevation data for each plot were generated from the SRTM 90-m spatial resolution digital elevation model (DEM) downloaded from USGS [50]. Moreover, the mean values from 6×6 pixel windows over the plots for each of the spectral variables were extracted to reduce the uncertainties of mapping forest AGB due to plot location and the uncertainties in RS data resulting from plot positioning errors. These errors included those introduced when the sample plots were located using GPS, X- and Y-UTM coordinates that were misleading, and sample plots that were mismatched with the image pixels [53]. Landsat spectral variables were extracted from image dates that closely approximated the years of the forest inventory plots to reduce spatial and temporal data mismatches between these datasets [54].

The AGB models for different land covers were developed using many available predictors, grouped into three distinct categories:

- Raw Landsat bands (B1–B5 and B7) as reflectance;
- VIs, including the simple ratio (SR), difference vegetation index (DVI), normalized difference vegetation index (NDVI), ratio vegetation index (RVI), global environmental monitoring index (GEMI), soil-adjusted vegetation index (SAVI), enhanced vegetation index (EVI), tasseled cap index of greenness (TCG), tasseled cap index of brightness (TCB), and tasseled cap index of wetness (TCW); and
- Topographically derived variables at a spatial resolution of 90 m, including elevation data generated from the SRTM 90-m digital elevation model (DEM) downloaded from the USGS.

Ten widely used indices associated with Landsat RS change detection and biomass estimation were used. The tested VIs consisted of the SR of the near infrared and red wavelengths; the DVI, which is a simple VI calculated as the difference between the infrared and red wavelengths; the NDVI, which is

the ratio of contrasting reflectance between the maximum absorption of the red wavelength due to chlorophyll pigments and the maximum reflectance of the infrared wavelength due to leaf cellular structure [55]; the RVI, which is a simple VI calculated by dividing the reflectance value of the near infrared wavelength by that of the red wavelength [56]; the GEMI, which is a non-linear VI similar to the NDVI but less sensitive to atmospheric affects; the SAVI, which is similar to the NDVI but adds a soil brightness correction factor [57,58]; the EVI, which was developed to address specific limitations of the NDVI by being more sensitive to changes in areas with high biomass and reducing the influence of atmospheric conditions on VIs; and the TCG, TCB, and TCW, which were derived directly from the raw Landsat bands using the reflectance-based transformation [59]. The TC components have been widely used to characterize vegetation conditions and forest change [59,60] (see Table 2 [58,61–65]). These indices can measure the presence and density of green vegetation, overall reflectance (e.g., differentiating light from dark soils), soil moisture content, and vegetation density (structure) [66]. We tested traditional indices and a variety of modified VIs because of their wide use in characterizing vegetation.

Table 2. The Landsat vegetation indices (Vis) used in this study.

VIs for Landsat Multi-Spectral Scanner (MSS) and TM		
Equation	Type of Index	Reference
$SR = \frac{TM4}{TM3}$	SR	Tucker [61]
$DVI = TM4 - TM3$	DVI	Tucker [61]
$NDVI = \frac{TM4 - TM3}{TM4 + TM3}$	NDVI	Tucker [61]
$RVI = \frac{TM3}{TM4}$	RVI	Pearson and Miller [62]
$GEMI = n(1 - 0.25n) \frac{TM3 - 0.125}{1 - TM3};$ $n = \frac{2(TM4^2 - TM3^2) + 1.5 \times TM4 + 0.5 \times TM3}{TM4 + TM3 + 0.5}$	GEMI	Pinty and Verstraete [63]
$SAVI = \frac{TM4 - TM3}{(TM4 + TM3 + 0.5)} \times (1 + 0.5)$	SAVI	Huete [58]
$EVI = 2.5 \times \frac{TM4 - TM3}{TM4 + 0.6 \times TM3 - 7.5 \times TM1 + 1}$	EVI	Huete <i>et al.</i> [64]
$TCG = -0.2848 \times TM1 - 0.2435 \times TM2 - 0.5436 \times TM3 +$ $0.7243 \times TM4 + 0.0840 \times TM5 - 0.1800 \times TM7$	TCG	Crist <i>et al.</i> [65]
$TCB = 0.3037 \times TM1 + 0.2793 \times TM2 + 0.4743 \times TM3 +$ $0.5585 \times TM4 + 0.5082 \times TM5 + 0.1863 \times TM7$	TCB	Crist <i>et al.</i> [65]
$TCW = 0.1509 \times TM1 + 0.1973 \times TM2 + 0.3279 \times TM3 +$ $0.3406 \times TM4 - 0.7112 \times TM5 - 0.4572 \times TM7$	TCW	Crist <i>et al.</i> [65]

A preliminary modeling step was used to define a suitable set of predictors for each model type. Thus, for each model type, three *a priori* models were constructed based on the unique variable permutations of the Landsat bands, the Landsat bands + spectral indices, and the Landsat bands + spectral indices + topographic variables (elevation). A stepwise regression analysis was used to select the best predictor from all variables correlated with AGB for each land-cover type. A multiple regression

model was used to identify the relationship between the AGB and RS data. Finally, the biomass estimation map for various land-cover types was generated from the models and land cover classification resulting from Section 2.4.

2.6. Model Validation

The models were evaluated using cross-validation by plot. For this analysis, the data were divided into two groups: the observed (y) and predicted (\hat{y}) values for each land-cover type. The AGB was the observed variable in these analyses. The RS data (e.g., TM bands, VIs, and elevation) were the predictors. The AGB predictions for each model were validated using a withheld validation dataset by calculating the RMSE between the observed and predicted values, as well as the relative RMSE, the bias, and the relative bias [54]. The results were validated by comparing the RMSE, the relative RMSE, the bias, and the relative bias of each model. Pearson correlation (r) was used to measure the strength of the linear relationship between variables. The probability value (p -value) was used to verify the performance of the model.

The RMSE and the relative RMSE were calculated using Equations (6) and (7), where (\hat{Y}_i) is the predicted AGB of the i th plot and (Y_i) is the observed AGB of the i th plot:

$$RMSE = \sqrt{\frac{\left(\hat{Y}_i - Y_i\right)^2}{n}} \quad (6)$$

$$RMSE\% = 100 \times \frac{RMSE}{\bar{Y}} \quad (7)$$

The bias and the relative bias were calculated from the difference between the mean predicted AGB ($\hat{\bar{Y}}$) and the mean observed AGB (\bar{Y}), as shown in Equations (8) and (9):

$$Bias = \hat{\bar{Y}} - \bar{Y} \quad (8)$$

$$Bias\% = 100 \times \frac{Bias}{\bar{Y}} \quad (9)$$

3. Results and Discussion

3.1. Vegetation Structure and Forest Composition

A total of 197 species were found in the DEF, MDF, and DDF sample sites (100, 91, and 105 species, respectively), and 38 species (21.2%) were found in all three forest types (including *Mitragyna rotundifolia* [Roxb.] Kuntze, *Irvingia malayana* Oliv. ex A. w. Benn., and *Millettia brandisiana* Kurz). A total of 23 species were found in the MDF and DDF sites, 7 species were found in the DEF and DDF sites, and 11 species were found in the DEF and MDF sites (see Figure 3). The dominant species in the DEF included *Lithocarpus polystachyus* (Wall.) Rehd., *Irvingia malayana* Oliv. ex A. w. Benn., and *Syzygium cumini* (L.) Skeels. The dominant species of the MDF were *Cananga odorata*, *Mitragyna rotundifolia* (Roxb.) Kuntze, and *Xylia sylocarpa* var. *kerrii* (Craib and Hutch.) I. Nielsen. The dominant species in the DDF were *Shorea obtusa* Wall. ex Blume, *Shorea siamensis* Miq.,

and *Cananga odorata*. The dominant species in the DF were *Cananga odorata*, *Tectona grandis* L.f., and *Shorea obtusa* Wall. ex Blume. The dominant species in the PFi were *Pterocarpus macrocarpus* Kurz, *Dipterocarpus tuberculatus* Roxb, and *Cananga odorata*.

Figure 3. The numbers of tree species in the predominant land-cover types in Savannakhet.

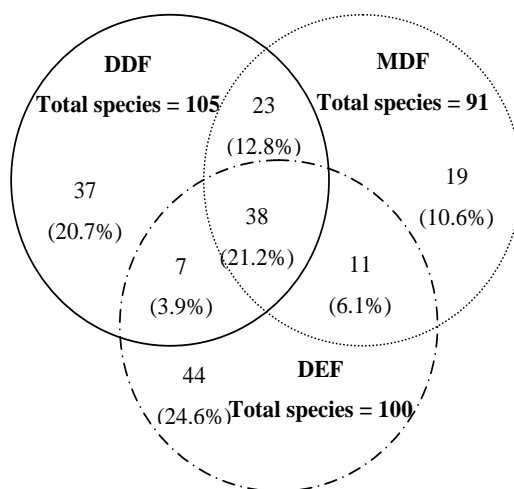


Table 3 shows the DBH, H, and average densities of the various land covers. The average tree densities per ha of the DEF, MDF, DDF, DF, and PFi were 805, 523, 605, 407, and 48, respectively; the average sapling densities per ha of these sites were 16,804, 7813, 9688, 4882, and 43, respectively. The average tree DBHs of the DEF, MDF, DDF, DF, and PFi sites were 11.19, 20.49, 13.31, 13.37, and 25.63, respectively, and the average sapling DBHs of these sites were 1.9, 2.05, 1.96, 2.05, and 0.29, respectively. The average tree H values of the DEF, MDF, DDF, DF, and PFi sites were 10.14, 12.40, 8.77, 7.58, and 9.55, respectively, and the average sapling H values of these sites were 3.58, 3.55, 2.77, 2.88, and 0.32, respectively.

Table 3. Average diameter at breast height (DBH), height (H), and density values of the trees and saplings for each land-cover type.

Vegetation Type	Land Cover	Avg. DBH (cm)	Avg. H (m)	Avg. Density (Number/ha)
Tree	DEF	11.19 (7.1–16.8)	10.14 (5.9–15.1)	805 (331–1469)
	MDF	20.49 (9.2–53)	12.4 (5.3–23)	523 (144–1269)
	DDF	13.31 (6.8–21.2)	8.77 (5.2–12.2)	605 (138–1238)
	DF	13.37 (5.5–30.3)	7.58 (3.4–15.3)	407 (19–1400)
	PFi	25.63 (10.9–39)	9.55 (5.5–16.4)	48 (6–100)
Sapling	DEF	1.9 (1.4–2.4)	3.58 (2.3–6.2)	16,804 (7031–32,344)
	MDF	2.05 (1.2–2.9)	3.55 (2.3–5)	7813 (156–18,125)
	DDF	1.96 (0–3.2)	2.77 (0–3.9)	9688 (0–32,656)
	DF	2.05 (1–3.6)	2.88 (1.8–6.8)	4882 (469–14,531)
	PFi	0.29 (0–3.2)	0.32 (0–3.5)	43 (0–469)

Note: The range is shown in parentheses.

The DEF had the highest average density for both trees and saplings, whereas the MDF had the highest average DBH for both trees and saplings. Although the average DBH of the PFi was highest, this site had the lowest tree density. The minimum DBH and H values of the saplings in the DDF and

PFi were 0 because several plots had no saplings. The MDF had the highest average H for trees, whereas the DEF had the highest average H for saplings. In this study, the DBH and H values of each individual tree and sapling in the plots were used to estimate the AGB following the allometric equation provided in Table 1.

3.2. AGB and Soil Carbon Analysis from Field Data

The data collected from the field were applied with the methodology described in Sections 2.2 and 2.3. The above-ground biomass and carbon stocks were largely influenced by the DBH, H, and density. A summary of the AGB and carbon stocks for various land covers is shown in Tables 4 and 5, and a summary of the soil carbon stock is shown in Table 6.

3.2.1. The AGB Analysis of Each Component from Field Data

Table 4 shows the results for the field data on the AGB of trees and saplings. The highest average AGB of trees in stems, branches, and leaves was found in the MDF, followed by the DEF, DDF, DF, and PFi. The results also showed that the highest average AGB in the stems, branches, and leaves of saplings belonged to the DEF, followed by DDF, MDF, DF, and PFi. The PFi had the lowest average AGB for all of the components of both trees and saplings.

Table 4. The AGB of each tree and sapling component by vegetation type.

Component	Land Cover	N	Avg. AGB (t/ha)	
			Tree	Sapling
Stem	DEF	11	46.04 (11.33–105.79)	3.49 (1.02–8.02)
	MDF	10	112.88 (13.16–447.12)	1.06 (0.03–2.5)
	DDF	20	37.17 (15.71–72.33)	1.18 (0–4.65)
	DF	29	22.58 (0.2–77.86)	0.52 (0.03–1.16)
	PFi	11	9.85 (0.68–55.24)	0.01 (0–0.11)
Branch	DEF	11	13.61 (3–32.41)	0.76 (0.22–1.75)
	MDF	10	29.06 (3.06–122.77)	0.14 (0–0.33)
	DDF	20	7.77 (2.93–15.8)	0.16 (0–0.6)
	DF	29	4.74 (0.03–17.43)	0.07 (0–0.15)
	PFi	11	2.21 (0.13–12.98)	0 (0–0.01)
Leaf	DEF	11	1.48 (0.57–2.86)	0.4 (0.14–0.89)
	MDF	10	2 (0.33–4.87)	0
	DDF	20	1.22 (0.41–2.28)	0
	DF	29	0.92 (0.01–6.12)	0.01 (0–0.09)
	PFi	11	0.29 (0.03–1.41)	0
Total	DEF	11	61.13 (14.91–141.06)	4.64 (1.38–10.66)
	MDF	10	143.95 (16.55–574.76)	1.19 (0.04–2.83)
	DDF	20	46.17 (19.25–90.34)	1.34 (0–5.26)
	DF	29	28.24 (0.24–97.53)	0.6 (0.03–1.41)
	PFi	11	12.34 (0.84–69.63)	0.01 (0–0.13)

Note: The range is shown in parentheses.

3.2.2. Total AGB Analysis of Land-Cover Types from Field Data

The total AGB was calculated from the trees, saplings, and undergrowth (*i.e.*, vegetation with H values less than 1.30 m, including seedlings, shrubs, climbers, grasses, litter (twigs and leaves), and paddies). These classes were defined based on their DBH and H values. The highest average total AGB for all sites was found for MDF, followed by DEF, DDF, DF, and PFi. Additionally, the PFi had the lowest average total AGB. Table 5 shows that 90% of the total AGB was composed of trees. The MDF had the highest AGB, whereas the PFi with scattered trees had the lowest AGB.

Table 5. The total biomass of trees, saplings, and undergrowth by vegetation type.

Types	Land Cover	N	Avg. Biomass (t/ha)
Tree	DEF	11	61.13 (14.91–141.06)
	MDF	10	143.95 (16.55–574.76)
	DDF	20	46.17 (19.25–90.34)
	DF	29	28.24 (0.24–97.53)
	PFi	11	12.34 (0.84–69.63)
Sapling	DEF	11	4.64 (1.38–10.66)
	MDF	10	1.19 (0.04–2.83)
	DDF	20	1.34 (0–5.26)
	DF	29	0.6 (0.03–1.32)
	PFi	11	0.01 (0–0.13)
Undergrowth	DEF	11	0.66 (0.22–1.43)
	MDF	10	1.45 (0.19–5.77)
	DDF	20	0.48 (0.21–0.91)
	DF	29	0.29 (0.01–0.98)
	PFi	11	0.12 (0.01–0.7)
Total	DEF	11	66.43 (22.51–144.45)
	MDF	10	146.59 (19.57–582.33)
	DDF	20	47.99 (21.45–91.84)
	DF	29	29.13 (0.77–98.77)
	PFi	11	12.48 (0.85–70.33)

Note: The range is shown in parentheses.

3.2.3. Soil Carbon Analysis from Field Data

The soil carbon stock was estimated to a depth of 30 cm because this depth is the most strongly affected by land management practices [46]. Soil carbon was analyzed based on bulk density and the soil carbon content percentage (see Table 6). The analysis showed that the MDF and DEF sites had the highest soil carbon content percentage at 1.03 and 0.98, respectively. The MDF site had the highest soil carbon stock, with an average of 40.17 t per ha, followed by the DEF, PFi, DF, and DDF sites. However, the soil carbon of the PFi site was high, suggesting that this paddy area was converted forest land [67]. Moreover, the use of fertilization increased the soil organic carbon density of the PFi site. The DF site had a higher soil carbon stock level than the DDF site because its forests had been disturbed and covered with grass that was high in soil organic carbon and contained an extensive fibrous root system that generated an ideal environment for soil microbial activity.

Table 6. Average soil carbon content by land-cover type.

Land Cover	Soil Sample Sites	Bulk Density (g/cm ³)	Soil Carbon Contents (%)	Estimated Soil Carbon (t/ha)
DEF	4	1.25	0.98 (0.95–1.01)	36.75 (35.625–37.875)
MDF	6	1.3	1.03 (0.99–1.08)	40.17 (38.61–42.12)
DDF	8	1.45	0.43 (0.3–0.69)	18.705 (13.05–30.015)
DF	8	1.52	0.58 (0.18–0.83)	26.448 (8.208–37.848)
PFi	8	1.78	0.67 (0.5–0.83)	35.778 (26.7–44.322)

Note: The range is shown in parentheses.

3.2.4. Carbon Stock Analysis from Field Data

The total carbon stock was estimated from the above-ground carbon stock, converted using Equation (7) and the soil carbon content (see Table 7). The MDF site had the highest carbon stock, followed by the DEF, PFi, DDF, and DF sites. The MDF had the highest above-ground carbon and soil carbon stock. The carbon stock of the DEF site was primarily in the soil rather than in the above-ground carbon because this site had the highest tree and sapling density and was high in soil organic carbon. The DF and PFi sites were higher in soil carbon than in above-ground carbon. The PFi site had the lowest above-ground carbon because it had fewer trees compared with the other land-cover types. The PFi site had a higher carbon stock than the DDF site because fertilization had previously increased the organic carbon density of the paddy soil. The DF site had a high soil carbon content because its forests had been disturbed. The site was covered with grass as a result of the disturbance. The grass was high in soil organic carbon and contained an extensive fibrous root system that generated an ideal environment for soil microbial activity.

Table 7. Average total carbon stock by land-cover type.

Land Cover	Above Ground (t/ha)		Soil Carbon (t/ha)	Total Carbon (t/ha)
	Biomass	Carbon		
DEF	65.77 (22.29–143.02)	30.91 (10.48–67.22)	36.75 (35.63–37.88)	67.66 (46.11–105.1)
MDF	145.14 (19.37–576.56)	68.22 (9.11–270.98)	40.17 (38.61–42.12)	108.39 (47.72–313.1)
DDF	47.51 (21.24–90.94)	22.33 (9.98–42.74)	18.71 (13.05–30.02)	41.04 (23.03–72.76)
DF	28.84 (0.76–97.79)	13.55 (0.36–45.96)	26.45 (8.21–37.85)	40 (8.57–83.81)
PFi	12.36 (0.84–69.63)	5.81 (0.4–32.73)	35.78 (26.7–44.32)	41.59 (27.1–77.05)

Note: The range is shown in parentheses.

The carbon biomass was highest in MDF and lowest in PFi (Table 8). The average carbon stock in DEF, MDF, DDF, DF, and PFi was 30.91, 68.22, 22.33, 13.55, and 5.81 (t/ha), respectively. A previous study in Kang Min Nho [68] found that the above-ground carbon stock of DEF, MDF, and DDF was 228.32, 156.53, and 152.65 (t/ha), respectively, based on direct measurements from the field. The results of the current study showed that carbon sequestration was considerably lower in Savannakhet than in Kang Min Nho. However, the results of this study are similar to the results obtained for carbon stock assessment in Thailand in 2007 and 2013 [69,70], and Lao in 2010 [71]. The carbon sequestration found by the current study was considerably less than that found by the Ogawa *et al.* study [40]. This result may suggest that the forests examined in the current study were

more strongly disturbed and affected by changes in the forestland. The studies also differed due to their initial times of study, site qualities, and carrying capacities for carbon sequestration. Furthermore, the tropical rain forest investigated in the current study was an immature forest. All of these factors potentially affected the differences between the results of the current study and the results of the Ogawa *et al.* study [40]. Additionally, Janmahasatien *et al.* [72] studied soil carbon in DEF and MDF at the Sa-kaerat environmental research station and at the Nakhon Ratchasima and Maeklong watershed stations. The current study found that soil organic carbon was 101.38 tC/ha in our DEF and 109.2 tC/ha in our MDF. To the best of our knowledge, no previous studies have investigated soil carbon in Laos according to forest types. Many factors, e.g., plant density and plant volume, affect above-ground biomass. The variables that control below-ground biomass include the soil type, bulk density, and forest cover.

Table 8. Carbon stock values in various forest types found by this study and by previous studies.

Country	Carbon Stock (t/ha)										Year	Reference
	DEF		MDF		DDF		DF		PFi			
	AG	Soil	AG	Soil	AG	Soil	AG	Soil	AG	Soil		
Lao PDR	30.91	36.75	68.22	40.17	22.33	18.71	13.55	26.45	5.81	35.78	2010	This study
Lao PDR	228.32	-	156.53	-	152.65	-	-	-	-	-	2013	[68]
Lao PDR	-	-	-	-	-	-	20	-	-	-	2010	[71]
Thailand	60.3	-	155.5	-	63	-	-	-	-	-	1965	[40]
Thailand	70.29	-	48.14	-	-	-	-	-	-	-	2007	[27]
Thailand	-	-	71.6	-	-	-	-	-	-	-	2007	[69]
Thailand	-	-	-	-	34.35	-	-	-	-	-	2013	[70]
Thailand		101.38		109.2	-	-	-	-	-	-	2007	[72]

3.3. RS-Based Biomass Model

3.3.1. Land-Cover Classification

The results obtained from the GIS data (e.g., land use) and the hybrid unsupervised and supervised classification techniques are shown in Figure 4. According to these results, the MDF and DDF sites had the highest coverage areas (624,553.06 and 518,210.50 ha, respectively). The DEF site had the lowest coverage area (198,932.81 ha), and the DF site covered a significant area (270,499.50 ha). Additionally, the PFi site covered a large area (308,188.44 ha). The rates of disturbance in the DEF, MDF, and DDF sites were high. Furthermore, most of the areas in the forest had been disturbed.

Based on the accuracy assessment using the hybrid classification, the overall accuracy was 82.56% (see Table 9). The results showed that PFi had the highest accuracy, followed by MDF, DEF, DDF, and DF. DF had the lowest accuracy because it had the greatest variation.

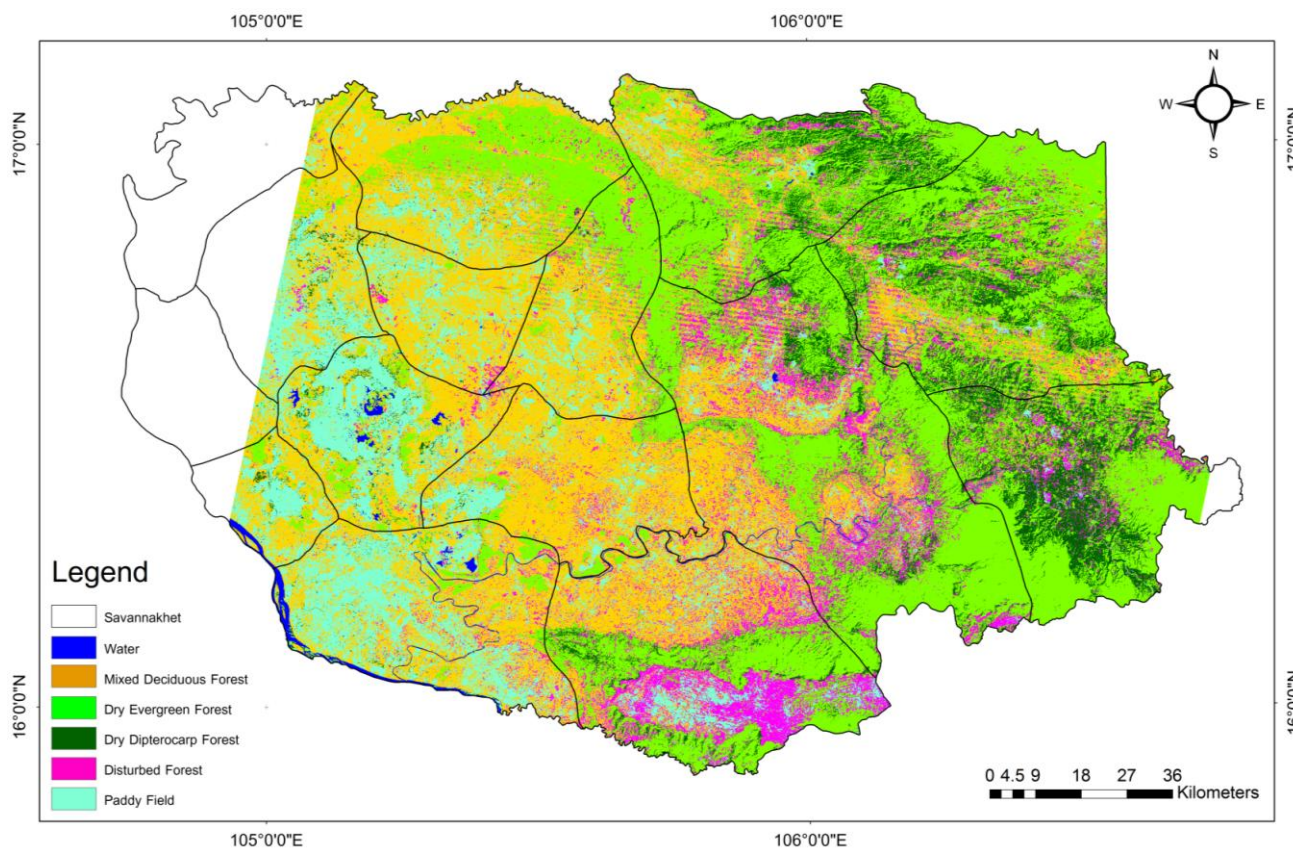
Table 9. The accuracy assessment of the hybrid land-cover classification technique.

Land Cover	DDF	MDF	DEF	DF	PFi	Water	Total	User's Accuracy (%)
DDF	69	8	0	12	7	0	96	71.88
MDF	6	114	9	8	1	2	140	81.43
DEF	0	2	14	2	0	0	18	77.78

Table 9. Cont.

Land Cover	DDF	MDF	DEF	DF	PFi	Water	Total	User's Accuracy (%)
DF	2	4	1	23	4	0	34	67.65
PFi	5	1	0	1	96	0	103	93.20
Water	0	0	0	0	0	39	39	100.00
Total	82	129	24	46	108	41	355	
Producer's Accuracy (%)	84.15	88.37	58.33	50.00	88.89	95.12		
Overall Accuracy							82.56	
Kappa							0.78	

Figure 4. Land-cover types in the Savannakhet area.



3.3.2. The AGB Regression Model

Linear regression models were developed using the previously described method. Comparisons of the regression coefficients among the different models based on a single TM band, single VI, elevation, or their combinations are presented in the Appendix. TM7 was the best single band and had the strongest regression coefficient for the DEF, with an R-value of 0.721. TM4 was the best single band for the MDF, DDF, and DF sites, with R-values of 0.504, 0.737, and 0.445, respectively. TM2 was the best single band for the PFi site, but it did not have a strong correlation. The VIs increasingly improved the relationship between the AGB and the spectral signature for the PFi site and slightly improved the relationship for the MDF. The analysis showed that a single TM band had a regression model that was sufficiently strong to allow the use of the model coefficients in developing biomass estimation models for the DEF and DDF sites but not for the MDF, DF, and PFi sites.

Therefore, two or more independent variables were required to improve the relationship between the AGB and the RS data. A stepwise regression analysis indicated that if the independent variables in the multiple regression models consisted of two or more TM bands, VIs, or other variables (e.g., elevation or a combination of the original independent variables), the regression coefficients significantly improved the R-values because high correlations were found among the spectral signatures, VIs, and the other variables. The results indicated that the RS data, including TM7, TM4, SR, DVI, RVI, SAVI, and elevation, were useful predictors of AGB for the DEF, MDF, DDF, DF, and PFi sites (Table 10). The DDF and MDF sites were strongly related to TM4 (in the near-infrared band), whereas the DEF site was strongly related to TM7 (in the MIR-infrared band). Moreover, the variable calculated from the RS data in multiple bands improved the correlation for the MDF, DDF, and PFi sites, and the elevation data improved the correlation for the MDF and DF sites.

The model was established based on field measurements, Landsat TM individual bands, various VIs, and the elevation data generated from the SRTM 90-m DEM downloaded from the USGS. Table 10 summarizes the best regression models for AGB estimation for each land-cover type in the study areas. The results of the model comparisons underscore the challenges posed by model validation and comparison. The plot-level validation revealed important but inconsistent differences between the five model types. In terms of R-value, RMSE, bias and relative bias, PFi performed best, but it exhibited the second weakest relative RMSE. In terms of bias and relative bias, the five models were similar, with MDF and PFi slightly positive and DEF, DDF, and DF slightly negative. In terms of *p*-value and relative RMSE, the DDF site was found to have the best and second highest RMSE, bias, and relative bias, whereas the DF site had the weakest R-value and relative RMSE but the third best RMSE, bias, and relative bias. MDF had the lowest RMSE and bias but the second highest R-value. The variable importance plot indicated that the combination of VIs explained the most variability in the AGB for the PFi site. Elevation was an important predictor for estimating AGB for the MDF and DF sites, and AGB tended to increase at higher elevations. The DF site was associated with the weakest correlation between the AGB and Landsat data. Most likely, this result was a consequence of the strong biophysical gradients that were correlated with biomass. The pattern within the DF site varied; for example, certain areas were strongly disturbed, whereas others were only slightly disturbed. In the linear model, the most significant relationships for the PFi site were found for RVI, SAVI, and SR, with an R-value of 0.931. The next most significant model for the MDF site was based on SR and elevation, with an R-value of 0.866. The third most significant model for the DDF site was based on TM4, with an R-value of 0.737. The fourth most significant model for the DEF site was based on TM7, with an R-value of 0.721. The weakest significant model for the DF site was based on TM4 and elevation, with an R-value of 0.595. These analyses and results implied that the use of a single TM band (TM7 or TM4) or a combination of variables (e.g., VIs and elevation) was successful for estimating AGB in the Savannakhet area. Additionally, the AGB estimates using the TM 4-5-3 color composite (Figure 1) showed that increased AGB is related to stronger vegetation growth stages. The total above-ground biomass and carbon stock for each land-cover type using the models is presented in Table 11. MDF had the highest AGB, 388.52 Mt, followed by DEF, DDF, DF, and PFi.

Table 10. Models used for AGB estimation (t/ha) for each land-cover type.

Models Used for AGB Estimation for Each Land-Cover Type							
Land Cover	Regression Models	R	p-Value	RMSE	Relative RMSE	Bias	Relative Bias
DEF	$AGB = 325.911 + (-10.816 \times TM7)$	0.721	0.012	24.95	37.93	-0.01	-0.02
MDF	$AGB = 202.406 + (196.558 \times SR) + (-1.884 \times \text{Elevation})$	0.866	0.027	81.87	54.58	0.07	0.05
DDF	$AGB = 101.633 + (-0.796 \times TM4)$	0.737	0.0003	14.07	29.64	-0.02	-0.05
DF	$AGB = -17.134 + (-0.816 \times TM4) + (0.550 \times \text{Elevation})$	0.595	0.015	19.72	68.39	-0.02	-0.08
PFi	$AGB = -1716.153 + (2071.324 \times RVI) + (1676.510 \times SAVI) + (-72.293 \times SR)$	0.931	0.002	6.9	55.89	0.001	0.008

Table 11. Total AGB and carbon stock estimation for each land-cover type.

Land Cover	Average AGB (t/ha)	Total AGB (Mt)	Total AG Carbon (Mt)
DEF	148.91(23.06–239.38)	32.91	15.47
MDF	388.52(113.8–587.73)	269.61	126.72
DDF	53.74(41.14–67.41)	30.94	14.54
DF	52.93(25.37–194.18)	15.91	7.48
PFi	37.42(2.77–134.51)	12.81	6.02
Total		362.18	170.22

3.3.3. Total Carbon Stock in the Study Area

The results of the carbon stock analysis are presented in Table 12 and Figure 5. This analysis found that the overall carbon stock was approximately 230.50 Mt, with an average of 120 t/ha. The MDF site had the highest total carbon stock, followed by the DDF and DEF site. The soil carbon content of the DEF, DF, and PFi sites was higher than their above-ground carbon stock (see Table 7). The DEF site had the highest density of trees (see Tables 4 and 5). In contrast, as the DF and PFi sites had small trees, the carbon stock at these sites was primarily in the soil and not in the above-ground trees. However, the MDF site was covered with large trees and had a lower density of trees than the DEF site. The soil and above-ground tree carbon stock at the DDF site were approximately the same, although the DDF site had larger trees than the DEF site; however, the DDF site also had fewer trees because of poor soil quality and illegal logging.

Table 12. The total carbon stock in Savannakhet Province, Lao People's Democratic Republic (PDR).

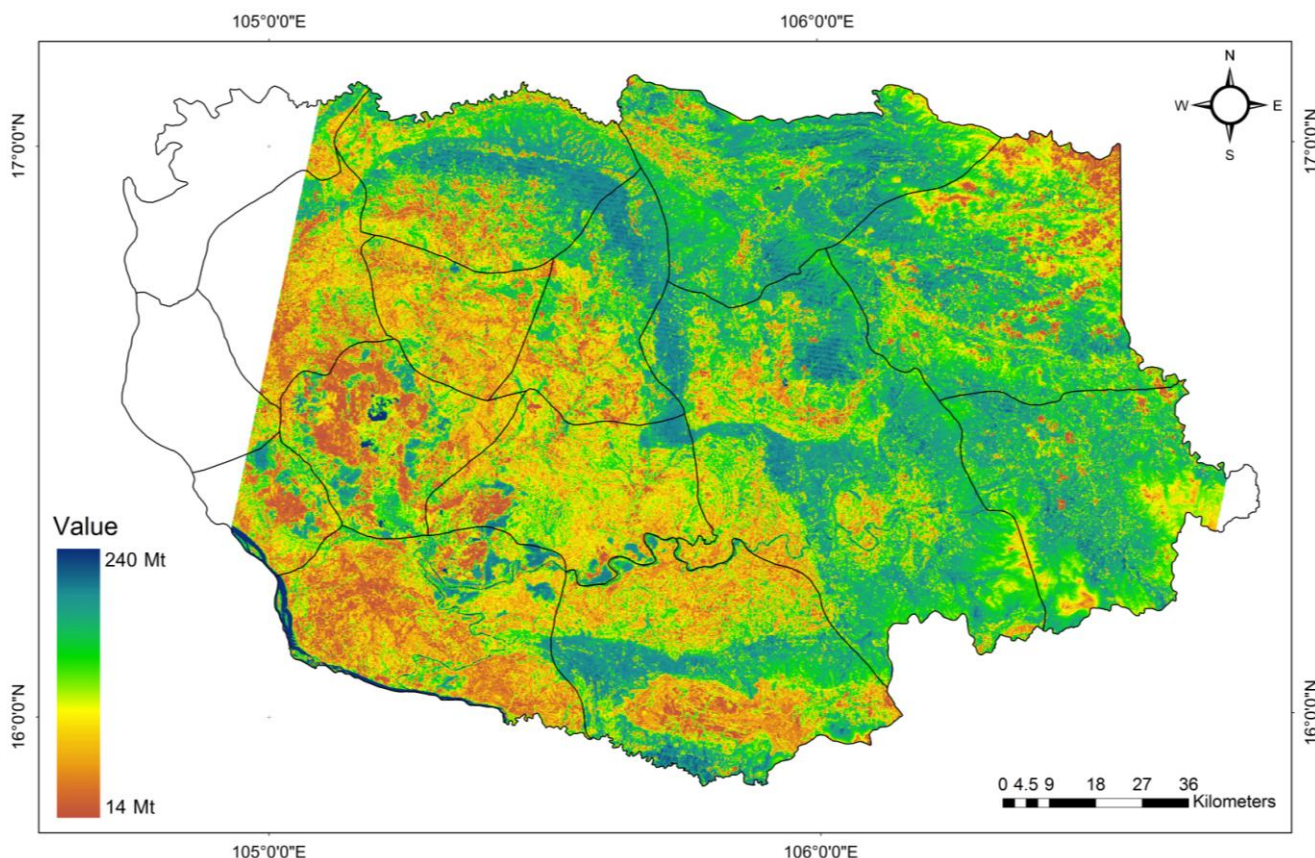
Land Cover	Area (ha)	Total (Mt)
DEF	198,932.81	22.78
MDF	624,553.06	151.80
DDF	518,210.50	24.23
DF	270,499.50	14.63

Table 12. Cont.

Land Cover	Area (ha)	Total (Mt)
PFi	308,188.44	17.05
Total	1,920,384.31	230.50

Note: The range is shown in parentheses.

Figure 5. Carbon stock map of Savannakhet area.



4. Conclusions

The results of the study showed a strong statistical relationship between the AGB and Landsat data. A linear regression analysis indicated that the strongest relationship was between the PFi site and the RS data, followed by the MDF, DDF, DEF, and DF sites. A significant correlation was found between the AGB and Landsat data (spectral reflectance, VIs, and elevation). The results of this study showed that TM7, TM4, SR, RVI, and SAVI were significantly and positively correlated with AGB in Savannakhet Province. Combinations of variables (e.g., Landsat TM band, VIs, and elevation) increased the correlations among the PFi, MDF, DF, and AGB, whereas single TM bands were strongly correlated with the DEF and DDF sites, as well as with the AGB. Given the accuracy of these estimates, the developed models successfully estimated the AGB for different land-cover types in Savannakhet Province and could be used to map the AGB in this area in the future.

However, this research mainly focuses on information of forest plot based measurement since forest stores large amount of carbon rather than other land cover. Therefore, carbon conversion factor of crop, e.g., paddy should be studied in greater details. Moreover, the factors affecting the reflectance of

this area should be studied more in the future including the effect of the undergrowth vegetation on the canopy reflectance in a continuum of canopy closure. Landsat data have been widely used in the study of forest due to the long run satellite data with free or low cost. A cost-effective approach would be very advantage for countries with limited above ground biomass data for developing allometric equations. However, the aboveground biomass estimation across the landscape can be improved by incorporating tree height as an additional driving variable using light detection and ranging (LiDAR) remote sensing technique [16,17].

Acknowledgments

The Greater Mekong Subregion Environment Operations Center (GMS-EOC), Asian Development Bank (ADB), Thailand funded this research. The authors acknowledge Prasong Thammapala for his advice and support. We thank the anonymous reviewers, whose comments improved this paper considerably.

Author Contributions

Phutchard Vicharnakorn, Rajendra P. Shrestha, Masahiko Nagai, Abdul P. Salam, and Somboon Kiratiprayoon developed the research concept and methods. Phutchard Vicharnakorn and the GMS-EOC teams collected and prepared the data. Phutchard Vicharnakorn conducted the research. Phutchard Vicharnakorn and Prasong Thammapala performed and interpreted the data analyses, which were then discussed with all of the authors. Phutchard Vicharnakorn wrote the manuscript with contributions from all of the authors.

Conflicts of Interest

The authors declare no conflict of interest.

References

1. Food and Agriculture Organization of the United Nations (FAO). *State of World's Forest*; Food FAO: Rome, Italy, 2011.
2. Gullison, R.E.; Frumhoff, P.C.; Canadell, J.G.; Field, C.B.; Nepstad, D.C.; Hayhoe, K.; Avissar, R.; Curran, L.M.; Friedlingstein, P.; Jones, C.D.; *et al.* Tropical forests and climate policy. *Science* **2007**, *316*, 985–986.
3. Intergovernmental Panel on Climate Change (IPCC). *Climate Change 2007: The Physical Science Basis: Working Group I Contribution to the Fourth Assessment Report of the IPCC*; Cambridge University Press: Cambridge, UK, 2007.
4. Brown, S. *Estimating Biomass and Biomass Change of Tropical Forests*; FAO Forest Resources Assessment Publication: Roma, Italy, 1997; p. 55.
5. Achard, F.; Eva, H.D.; Stibig, H.; Mayaux, P.; Gallego, J.; Richards, T.; Malingreau, J. Determination of deforestation rates of the World's humid tropical forests. *Science* **2002**, *297*, 999–1002.

6. Mokany, K.; Raison, J.R.; Prokushkin, A.S. Critical analysis of root-shoot ratios in terrestrial biomes. *Glob. Chang. Biol.* **2006**, *12*, 84–96.
7. Houghton, R.A.; Hall, F.; Goetz, S. Importance of biomass in the global carbon cycle. *J. Geophys. Res.* **2009**, *114*, 1–13.
8. International Conference on Emergency Medicine (ICEM). Lao PDR National Report on Protected Areas and Development. In *Review of Protected Areas and Development in the Lower Mekong River Region*; ICEM: Indooroopilly, QLD, Australia, 2003; p. 101.
9. Attarchi, S.; Gloaguen, R. Improving of above ground biomass using dual polarimetric PALSAR and ETM+ data in the Hyrcanian forest (Iran). *Remote Sens.* **2014**, *6*, 3693–3715.
10. Maynard, C.L.; Lawrence, R.L.; Nielsen, G.A.; Decker, G. Modeling vegetation amount using bandwise regression and ecological site descriptions as an alternative to vegetation indices. *GISci. Remote Sens.* **2007**, *44*, 68–81.
11. Main-Knorn, M.; Moisen, G.G.; Healey, S.P.; Keeton, W.S.; Freeman, E.A.; Hostert, P. Evaluating the remote sensing and inventory-based estimation of biomass in the Western Carpathians. *Remote Sens.* **2011**, *3*, 1427–1446.
12. Neigh, C.S.R.; Bolton, D.K.; Diabate, M.; Williams, J.J.; Carvalhais, N. An automated approach to map the history of forest disturbance from insect mortality and harvest with Landsat Time-Series data. *Remote Sens.* **2014**, *6*, 2782–2808.
13. Lu, D. The potential and challenge of remote sensing-based biomass estimation. *Int. J. Remote Sens.* **2006**, *27*, 1297–1328.
14. Ramankutty, N.; Gibbs, H.K.; Achard, F.; DeFries, R.; Foley, J.A.; Houghton, R.A. Challenges to estimating carbon emissions from tropical deforestation. *Glob. Chang. Biol.* **2007**, *13*, 51–66.
15. Somphone, C. Participatory Forest Management: A Research Study in Savannakhet Province, Laos. In *Laos Country Report 2003*; Institute for Global Environmental Strategies: Kanagawa, Japan, 2004; pp. 44–45.
16. Kankare, V.; Vastaranta, M.; Holopainen, M.; Raty, M.; Yu, X.; Hyypä, J.; Hyypä, H.; Alho, P.; Viitala, R. Retrieval of forest aboveground biomass and stem volume with airborne scanning LiDAR. *Remote Sens.* **2013**, *5*, 2257–2274.
17. Wannasiri, W.; Masahiko, N.; Kiyoshi, H.; Santitamnont, P.; Miphokasap, P. Extraction of mangrove biophysical parameters using Airborne LiDAR. *Remote Sens.* **2013**, *5*, 1787–1808.
18. Foody, G.M.; Boyd, D.S.; Cutler, M.E.J. Predictive relations of tropical forest biomass from Landsat TM data and their transferability between regions. *Remote Sens. Environ.* **2003**, *85*, 463–474.
19. Kobayashi, S.; Omura, Y.; Sanga-Ngoie, K.; Widyorini, R.; Kawai, S.; Supriadi, B.; Yamaguchi, Y. Characteristics of decomposition powers of L-band multi-polarimetric SAR in assessing tree growth of industrial plantation forest in the tropics. *Remote Sens.* **2012**, *4*, 3058–3077.
20. Clewley, D.; Lucas, R.; Accad, A.; Armston, J.; Bowen, M.; Dwyer, J.; Pollock, S.; Bunting, P.; McAlpine, C.; Eyre, T.; *et al.* An approach to mapping forest growth stages in Queensland, Australia through Integration of ALOS PALSAR and Landsat sensor data. *Remote Sens.* **2012**, *4*, 2236–2255.

21. Robinson, C.; Saatchi, S.; Neumann, M.; Gillespie, T. Impacts of spatial variability on aboveground biomass estimation from L-band Radar in a temperate forest. *Remote Sens.* **2013**, *5*, 1001–1023.
22. Zheng, D.; Rademacher, J.; Chen, J.; Crow, T.; Bresee, M.; Le Moine, J.; Ryu, S. Estimating aboveground biomass using Landsat 7 ETM+ data across a managed landscape in Northern Wisconsin, USA. *Remote Sens. Environ.* **2004**, *93*, 402–411.
23. Coulibaly, L.; Migolet, P.; Adegbedi, G.H.; Fournier, R.; Hervet, E. Mapping Aboveground Forest Biomass from IKONOS Satellite Image and Multi-Source Geospatial Data Using Neural Networks and a Kriging Interpolation. In Proceedings of IEEE International Geoscience and Remote Sensing Symposium, 2008 (IGARSS 2008), Boston, MA, USA, 7–11 June 2008; pp. 298–301.
24. Castel, T.; Guerra, F.; Caraglio, Y.; Houllier, F. Retrieval biomass of a large Venezuelan pine plantation using JERS-1 SAR data. Analysis of forest structure impact on radar signature. *Remote Sens. Environ.* **2002**, *79*, 30–41.
25. Wijaya, A.; Gloaguen, R. Fusion of ALOS Palsar and Landsat ETM Data for Land Cover Classification and Biomass Modeling Using Non-Linear Methods. In Proceedings of IEEE International Geoscience and Remote Sensing Symposium, 2009 (IGARSS 2009), Cape Town, South Africa 12–17 June 2009; pp. 581–584.
26. Anindya, M.K.; Yadavand, N. Applying enhanced k-Nearest neighbor approach on satellite images for forest biomass estimation of Vellore district. *Eng. Sci. Technol. Int. J.* **2012**, *2*, 2250–3498.
27. Terakunpisut, J.; Gajasen, N.; Ruankawe, N. Carbon sequestration potential in aboveground biomass of Thong Pha Phum National Forest, Thailand. *Appl. Ecol. Environ. Res.* **2007**, *5*, 93–102.
28. Schlerf, M.; Alzberger, C.; Hill, J. Remote sensing of forest biophysical variables using HyMap imaging spectrometer data. *Remote Sens. Environ.* **2005**, *95*, 177–194.
29. Das, S.; Singh, T.P. Correlation analysis between biomass and spectral vegetation indices of forest ecosystem. *Int. J. Eng. Res. Technol.* **2012**, *1*, 1–13.
30. Patel, N.K.; Saxena, R.K.; Shiwalkar, A. Study of fractional vegetation cover using high spectral resolution data. *J. Indian Soc. Remote Sens.* **2007**, *35*, 73–79.
31. Zhang, C.; Franklin, S.E.; Wulder, M.A. Geostatistical and texture analysis of Airborne acquired images used in forest classification. *Int. J. Remote Sens.* **2004**, *25*, 859–865.
32. Samaniego, L.; Schulz, K. Supervised classification of agricultural land cover using a modified k-NN technique (MNN) and Landsat remote sensing imagery. *Remote Sens.* **2009**, *1*, 875–895.
33. Labrecque, S.; Fournier, R.; Luther, J.; Piercy, D. A comparison of four methods to maps biomass from Landsat-TM and inventory data in western Newfoundland. *For. Ecol. Manag.* **2006**, *226*, 129–144.
34. Ohmann, J.L.; Gregory, M.J. Predictive mapping of forest composition and structure with direct gradient analysis and nearest-neighbor imputation in coastal Oregon, USA. *Canadian. J. For. Res.* **2002**, *32*, 725–741.
35. Kamusoko, C.; Aniya, M. Hybrid classification of Landsat data and GIS for land use/cover change analysis of the Bindura district, Zimbabwe. *Int. J. Remote Sens.* **2009**, *30*, 97–115.

36. Yuan, F.; Bauer, M.E.; Heinert, N.J.; Holden, G. Multi-level Land Cover Mapping of the Twin Cities (Minnesota) Metropolitan area with multi-seasonal Landsat TM/ETM+ Data. *Geocarto Int.* **2005**, *20*, 5–14.
37. Food and Agriculture Organization of the United Nations (FAO). National Forest Products Statistics, Lao PDR. In *An Overview of Forest Products Statistics in South and Southeast Asia: Forestry Statistics and Data Collection*; FAO: Bangkok, Thailand, 2002; pp. 117–184.
38. Committee for Planning and Cooperation. The National Committee for Poverty Eradication. In *The National Poverty Eradication Programme*; Committee for Planning and Cooperation: Vientiane, Laos, 2003.
39. Tsutsumi, T.; Yoda, K.; Sahunalu, P.; Dhanmanonda, P.; Prachaiyo, B. Chapter 3. Shifting Cultivation: An Experiment at Nam Phrom, Northeast Thailand and Its Implications for Upland Farming in the Monsoon Tropics. In *Forest: Felling, Burning and Regeneration*; Kyoto University: Kyoto, Japan, 1983; pp. 13–62.
40. Ogawa, H.; Yoda, K.; Ogino, K.; Kira, T. Comparative ecological studies on three main type of forest vegetation in Thailand II. *Plant Biomass Nat. Life Southeast Asia* **1965**, *4*, 49–80.
41. Visaratana, T.; Chernkhuntod, C. *Species and above Ground Biomass of Dry Evergreen Forest*; Department of National Park, Wildlife, and Plant Conservation, Kasetsart University: Bangkok, Thailand, 2004.
42. Suwannapinunt, W. A study on the biomass of *Thyrsostachys siamensis* GAMBLE forest at Hin-Lap, Kanchanaburi. *J. Bamboo Res.* **1983**, *2*, 82–101.
43. Glumphabut, P.; Kaitpraneet, S.; Wachrinrat, C. Nutrient dynamics of natural evergreen forests in the eastern region of Thailand. *Kasetsart J. Nat. Sci.* **2007**, *41*, 811–822.
44. Chaiyo, U.; Garivait, S.; Wanthongchai, K. Structure and carbon storage in aboveground biomass of mixed deciduous forest in western region, Thailand. *GMSARN Int. J.* **2012**, *6*, 143–150.
45. Sempaseuth, P.; Navanugraha, C.; Pattanakiat, S. The estimation of carbon storage in dry evergreen and dry dipterocarp forest in Sang Khom District, Nong Khai province, Thailand. *Environ. Nat. Resour. J.* **2009**, *7*, 1–11.
46. Powers, J.S.; Corre, M.D.; Twine, T.E.; Veldkamp, E. Geographic bias of field observations of soil carbon stocks with tropical land-use changes precludes spatial extrapolation. *Biol. Sci.* **2011**, *108*, 6318–6322.
47. Vagen, T.G.; Winowiecki, L.A. Mapping of soil organic carbon stocks for spatially explicit assessments of climate change mitigation potential. *Environ. Res. Lett.* **2013**, *8*, 1748–1793.
48. Grossman, R.B.; Reinsch, T.G. The Solid Phase: 2.1. In *Bulk Density and Linear Extensibility: Methods of Soil Analysis, Part 4*; Soil Science Society of America Madison: Madison, WI, USA, 2002; pp. 201–225.
49. Black, C.A. Hydrogen-ion Activity. In *Methods of Soil Analysis Part II: Chemical and Microbiological Properties*; America Society of Agronomy: Madison, WI, USA, 1965; pp. 771–1572.
50. U.S. Geological Survey. Earth Resources Observation and Science Center (EROS). Available online: <http://glovis.usgs.gov/> (accessed on 29 January 2014).
51. Pradhan, R.; Ghose, M.K.; Jeyaram, A. Land cover classification of remotely sensed satellite data using Bayesian and Hybrid classifier. *Int. J. Comput. Appl.* **2010**, *7*, 1–4.

52. Bahadur, K. Improving Landsat and IRS image classification: Evaluation of unsupervised and supervised classification through band ratios and DEM in a mountainous landscape in Nepal. *Remote Sens.* **2009**, *1*, 1257–1272.
53. Lu, D.; Mausel, P.; Brondizio, E.; Moran, E. Assessment of atmospheric correction methods for Landsat TM data applicable to Amazon basin LBA research. *Int. J. Remote Sens.* **2002**, *23*, 2651–2671.
54. Wang, G.; Zhang, M.; Gertner, G.Z.; Oyana, T.; McRoberts, R.E.; Ge, H. Uncertainties of mapping aboveground forest carbon due to plot locations using national forest inventory plot and remotely sensed data. *Scand. J. For. Res.* **2011**, *26*, 360–373.
55. Powell, S.L.; Cohen, W.B.; Healey, S.P.; Kennedy, R.E.; Gretchen, G.M.; Pierce, K.B.; Ohmann, J.L. Quantification of live aboveground forest biomass dynamics with Landsat time-series and field inventory data: A comparison of empirical modeling approaches. *Remote Sens. Environ.* **2010**, *114*, 053–1068.
56. Piao, S.L.; Fang, J.Y.; Zhou, L.M.; Tan, K.; Tao, S. Changes in biomass carbon stocks in China's grasslands between 1982 and 1999. *Glob. Biogeochem. Cycles* **2007**, *21*, 1–10.
57. Richardson, A.J.; Wiegand, C.L. Distinguishing vegetation from soil background information. *Photogramm. Eng. Remote Sens.* **1977**, *43*, 1541–1552.
58. Huete, A.R. A soil-adjusted vegetation index (SAVI). *Remote Sens. Environ.* **1988**, *25*, 295–309.
59. Crist, E.P. A TM tasseled cap equivalent transformation for reflectance factor data. *Remote Sens. Environ.* **1985**, *17*, 301–306.
60. Healey, S.P.; Cohen, W.B.; Yang, Z.; and Krankina, O.N. Comparison of Tasseled Cap-based Landsat data structures for forest disturbance detection. *Remote Sens. Environ.* **2005**, *97*, 301–310.
61. Tucker, C.J. Red and photographic infrared linear combinations for monitoring vegetation. *Remote Sens. Environ.* **1979**, *8*, 127–150.
62. Pearson, R.L.; Miller, D.L. Remote Mapping of Standing Crop Biomass for Estimation of the Productivity of the Short-Grass Prairie, Pawnee National Grassland, Colorado. In Proceedings of the Eighth International Symposium on Remote Sensing of Environment, Michigan, MI, USA, 2–6 October 1972; pp. 1357–1381.
63. Pinty, B.; Verstraete, M.M. GEMI: A non-linear index to monitor global vegetation from satellites. *Vegetation* **1992**, *101*, 15–20.
64. Huete, A.; Keita, F.; Thome, K.; Privette, J.; Van Leeuwen, W.J.D.; Justice, C.; Morisette, J.A. Light aircraft radiometric package for MODLAND Quick Airborne Looks (MQUALS). *Earth Obs.* **1999**, *11*, 22–25.
65. Crist, E.P.; Laurin, R.; Cicone, R.C. Vegetation and Soils Information Contained in Transformed Thematic Mapper Data. In Proceedings of 1986 International Geoscience and Remote Sensing Symposium (IGARSS' 86) on Remote Sensing, Zurich, Switzerland, 8–11 September 1986; pp. 1465–1470.
66. Cohen, W.B.; Goward, S.N. Landsat's role in ecological applications of remote sensing. *Bioscience* **2004**, *54*, 535–545.
67. Forestry Department Food and Agriculture Organization of the United Nations (FRA). *Global Forest Resources Assessment 2010 Country Report Lao People's Democratic Republic*; Forestry FRA: Rome, Italy, 2010.

68. Kang, M.N. *Forest Cover and Carbon Mapping in the Greater Mekong Subregion and Malaysia*; The Third Progress Workshop: Beijing, China, 2013.
69. Petsri, S.; Pumijumnong, N. Aboveground carbon content in mixed deciduous forest and teak plantation. *Environ. Natl. Resour. J.* **2007**, *5*, 1–10.
70. Homchan, C.; Khamyong, S.; Anongrak, N. Plant Diversity and Biomass Carbon Storage in a Dry Dipterocarp Forest with Planted Bamboos at Huai Hong Krai Royal Development Study Center, Chiang Mai Province. In Proceedings of the International Graduate Research Conference, Chiang Mai University, Chiang Mai, Thailand, 20 December 2013.
71. Reduced Emissions from Deforestation and Forest Degradation. *REDD Concept Note, Biodiversity Corridor VietNam ADBR-PPTA 7459: GMS Biodiversity Conservation Corridors*; National University of Laos: Laos, Vientiane, Thailand, 2010.
72. Janmahasatien, S.; Phopinit, S.; Wichienopparat, W. *Soil Carbon in the Sakaerat Dry Evergreen Forest and the Maeklong Mixed Deciduous Forest*; Department of National Parks, Wildlife, and Plant Conservation: Bangkok, Thailand, 2007.

Appendix

Table A1. Correlation between RS variables and AGB.

Land Cover	Independent Variable	Constant	Coefficient	R	p-Value	
DEF	TM Bands	TM1	123.855	−1.255	0.366	0.268
		TM2	200.799	−5.033	0.329	0.323
		TM3	164.703	−5.016	0.31	0.354
		TM4	49.622	0.185	0.144	0.673
		TM5	212.605	−1.941	0.424	0.194
		TM7	325.911	−10.816	0.721	0.012
		VIs	SR	41.63	5.311	0.23
	DVI		52.466	0.197	0.161	0.637
	NDVI		44.322	36.591	0.203	0.549
	RVI		74.483	−30.21	0.185	0.585
	GEMI		59.449	0.001	0.104	0.762
	SAVI		44.346	24.476	0.203	0.549
	EVI		53.628	−3.323	0.198	0.559
	TCG		55.742	0.289	0.192	0.571
	TCB		101.013	−0.288	0.109	0.751
	TCW	90.012	1.48	0.383	0.244	
MDF	Topographic	Elevation	18.086	0.145	0.312	0.351
	TM Bands	TM1	−45.634	3.203	0.163	0.654
		TM2	103.076	1.599	0.031	0.931
		TM3	84.647	2.586	0.117	0.748
		TM4	−7.797	2.92	0.504	0.137
		TM5	402.993	−3.102	0.198	0.584
		TM7	160.067	−0.359	0.018	0.96
	VIs	SR	−131.759	138.281	0.69	0.027

Table A1. Cont.

Land Cover	Independent Variable	Constant	Coefficient	R	p-Value			
DDF	Topographic TM Bands	DVI	29.349	4.193	0.586	0.075		
		NDVI	-23.569	590.49	0.65	0.055		
		RVI	414.139	-458.119	0.622	0.056		
		GEMI	57.203	0.068	0.581	0.078		
		SAVI	-23.013	394.673	0.694	0.042		
		EVI	39.471	-358.781	0.544	0.104		
		TCG	132.285	6.638	0.614	0.059		
		TCB	-71.973	1.92	0.301	0.398		
		TCW	403.099	8.689	0.605	0.064		
		Elevation	242.599	-0.385	0.122	0.736		
		TM1	11.748	0.613	0.265	0.273		
		TM2	110.203	-2.111	0.297	0.217		
		TM3	81.724	-1.361	0.292	0.225		
		TM4	101.633	-0.796	0.737	0.0003		
		TM5	50.954	-0.045	0.021	0.931		
		TM7	46.938	0.02	0.005	0.984		
		DF	VIs	SR	82.694	-12.828	0.536	0.018
				DVI	83.058	-0.829	0.717	0.001
				NDVI	101.001	-121.166	0.634	0.004
				RVI	-3.662	129.432	0.697	0.001
				GEMI	65.501	-0.008	0.666	0.002
				SAVI	100.901	-81.064	0.594	0.007
				EVI	61.109	19.455	0.566	0.011
TCG	60.642			-0.966	0.684	0.001		
TCB	143.592			-0.798	0.56	0.013		
TCW	23.501			-1.126	0.517	0.023		
DF	Topographic TM Bands			Elevation	-82.038	0.645	0.439	0.06
				TM1	-10.123	0.644	0.234	0.221
				TM2	31.381	-0.081	0.015	0.937
				TM3	34.893	-0.237	0.055	0.778
				TM4	96.32	-0.846	0.445	0.015
		TM5	40.879	-0.135	0.104	0.591		
		TM7	32.519	-0.115	0.053	0.784		
		VIs	SR	57.476	-8.613	0.314	0.097	
			DVI	68.09	-0.724	0.401	0.031	
			NDVI	67.291	-75.413	0.298	0.116	
			RVI	1.097	83.44	0.37	0.048	
			GEMI	47.979	-0.006	0.373	0.046	
			SAVI	67.388	-50.646	0.271	0.155	
			EVI	44.601	19.81	0.402	0.031	
			TCG	46.782	-0.868	0.405	0.029	
TM7	160.067	-0.359	0.018	0.96				

Table A1. Cont.

Land Cover	Independent Variable	Constant	Coefficient	R	p-Value		
DDF	VIs	SR	-131.759	138.281	0.69	0.027	
		DVI	29.349	4.193	0.586	0.075	
		NDVI	-23.569	590.49	0.65	0.055	
		RVI	414.139	-458.119	0.622	0.056	
		GEMI	57.203	0.068	0.581	0.078	
		SAVI	-23.013	394.673	0.694	0.042	
		EVI	39.471	-358.781	0.544	0.104	
		TCG	132.285	6.638	0.614	0.059	
		TCB	-71.973	1.92	0.301	0.398	
		TCW	403.099	8.689	0.605	0.064	
	Topographic TM Bands	Elevation	242.599	-0.385	0.122	0.736	
		TM1	11.748	0.613	0.265	0.273	
		TM2	110.203	-2.111	0.297	0.217	
		TM3	81.724	-1.361	0.292	0.225	
		TM4	101.633	-0.796	0.737	0.0003	
		TM5	50.954	-0.045	0.021	0.931	
		TM7	46.938	0.02	0.005	0.984	
		VIs	SR	82.694	-12.828	0.536	0.018
			DVI	83.058	-0.829	0.717	0.001
			NDVI	101.001	-121.166	0.634	0.004
RVI	-3.662		129.432	0.697	0.001		
GEMI	65.501		-0.008	0.666	0.002		
SAVI	100.901		-81.064	0.594	0.007		
EVI	61.109		19.455	0.566	0.011		
TCG	60.642		-0.966	0.684	0.001		
TCB	143.592		-0.798	0.56	0.013		
TCW	23.501		-1.126	0.517	0.023		
DF	Topographic TM Bands	Elevation	-82.038	0.645	0.439	0.06	
		TM1	-10.123	0.644	0.234	0.221	
		TM2	31.381	-0.081	0.015	0.937	
		TM3	34.893	-0.237	0.055	0.778	
		TM4	96.32	-0.846	0.445	0.015	
		TM5	40.879	-0.135	0.104	0.591	
		TM7	32.519	-0.115	0.053	0.784	
	VIs	SR	57.476	-8.613	0.314	0.097	
		DVI	68.09	-0.724	0.401	0.031	
		NDVI	67.291	-75.413	0.298	0.116	
		RVI	1.097	83.44	0.37	0.048	
		GEMI	47.979	-0.006	0.373	0.046	
		SAVI	67.388	-50.646	0.271	0.155	
		EVI	44.601	19.81	0.402	0.031	
		TCG	46.782	-0.868	0.405	0.029	

Table A1. Cont.

Land Cover	Independent Variable	Constant	Coefficient	R	p-Value		
PFi		TCB	70.735	−0.31	0.221	0.25	
		TCW	28.632	−0.008	0.005	0.979	
	Topographic	Elevation	−87.027	0.574	0.412	0.026	
	TM Bands	TM1	−21.89	0.562	0.303	0.365	
		TM2	38.16	−0.762	0.154	0.652	
		TM3	29.51	−0.556	0.206	0.544	
		TM4	60.606	−0.609	0.647	0.031	
		TM5	28.145	−0.174	0.115	0.731	
		TM7	27.007	−0.444	0.207	0.541	
		VIs	SR	34.562	−8.333	0.433	0.184
			DVI	41.743	−0.608	0.609	0.047
			NDVI	51.703	−93.096	0.612	0.045
			RVI	−30.766	103.482	0.616	0.043
			GEMI	25.165	−0.005	0.464	0.15
			SAVI	51.63	−62.232	0.426	0.191
			EVI	23.573	12.683	0.43	0.187
			TCG	23.94	−0.695	0.58	0.061
			TCB	72.31	−0.431	0.434	0.182
			TCW	−1.596	−0.524	0.271	0.42
		Topographic	Elevation	−125.23	0.75	0.506	0.112

© 2014 by the authors; licensee MDPI, Basel, Switzerland. This article is open access, distributed under the terms and conditions of the Creative Commons Attribution license (<http://creativecommons.org/licenses/by/3.0/>).